energies

MDPI

Article

Modeling and Investigation of the Effect of a Wind Turbine on the Atmospheric Boundary Layer

Vladislav N. Kovalnogov, Ruslan V. Fedorov *, Andrei V. Chukalin, Ekaterina V. Tsvetova and Mariya I. Kornilova

Laboratory of Inter-Disciplinary Problems in Energy Production, Ulyanovsk State Technical University, 32 Severny Venetz Street, 432027 Ulyanovsk, Russia

* Correspondence: r.fedorov@ulstu.ru

Abstract: Wind power engineering is one of the environmentally safe areas of energy and certainly makes a significant contribution to the fight against CO_2 emissions. The study of the air masses movement in the zone of wind turbines and their influence on the boundary layer of the atmosphere is a fundamental basis for the efficient use of wind energy. The paper considers the theory of the movement of air masses in the rotation zone of a wind turbine, and presents an analytical review of applied methods for modeling the atmospheric boundary layer and its interaction with a wind turbine. The results of modeling the boundary layer in the wind turbine zone using the STAR CCM+ software product are presented. The wind speed and intensity of turbulence in the near and far wake of the wind turbine at nominal load parameters are investigated. There is a significant decrease in the average wind speed in the near wake of the wind generator by 3 m/s and an increase in turbulent intensity by 18.3%. When considering the long-distance track behind the wind turbine, there is a decrease in the average speed by 0.6 m/s, while the percentage taken from the average value of the turbulent intensity is 7.2% higher than in the section in front of the wind generator. The influence of a wind turbine on the change in the temperature stratification of the boundary layer is considered. The experiments revealed a temperature change (up to 0.5 K), which is insignificant, but at night the stratification reaches large values due to an increase in the temperature difference in the surface boundary layer. In the long term, the research will contribute to the sustainable and efficient development of regional wind energy.

Keywords: mathematical modeling; computational fluid dynamics; turbulence; StarCCM+; wind farm; atmospheric boundary layer

check for updates

Citation: Kovalnogov, V.N.; Fedorov, R.V.; Chukalin, A.V.; Tsvetova, E.V.; Kornilova, M.I. Modeling and Investigation of the Effect of a Wind Turbine on the Atmospheric Boundary Layer. *Energies* **2022**, *15*, 8196. https://doi.org/10.3390/en15218196

Academic Editors: Chongyuan Zhang, Rui Wang and Bisheng Wu

Received: 14 September 2022
Accepted: 1 November 2022
Published: 3 November 2022

Publisher's Note: MDPI stays neutral with regard to jurisdictional claims in published maps and institutional affiliations.

Copyright: © 2022 by the authors. Licensee MDPI, Basel, Switzerland. This article is an open access article distributed under the terms and conditions of the Creative Commons Attribution (CC BY) license (https://creativecommons.org/licenses/by/4.0/).

1. Introduction

Wind energy is one of the most promising energy sources, confirmed by a significant increase in the capacity of wind power plants around the world [1,2]. In 2021 alone, 94 GW of capacity was put into operation; this is the second record year for the commissioning of capacity, only 1.8% less than the record indicator of 2020. Wind farms occupy large areas; thus, in this regard, the issue of the impact of wind farms on the boundary layer of the atmosphere and the environment becomes relevant. This work is aimed at studying the interaction of a wind turbine with the thermodynamic boundary layer of the atmosphere. In the long term, this will contribute to the sustainable development of regional wind energy. Wind turbines convert part of the kinetic energy flowing through the wind farm into electrical energy, while another part is converted into turbulence energy and the remainder leaves the wind farm as a reduced amount of kinetic energy. When considering a single wind turbine, its effect on the air flow from the upwind and downwind sides can be noted. The upwind side is also called the induction region, where a decrease in velocity is observed [3,4]. The area on the upwind side of the turbine is called the wake [5], which can be divided into near and far wakes (Figure 1).

The near wake is characterized by high turbulence and the greatest change in the velocity gradient. The near wake can reach up to four diameters of the main rotor according to the profile of the blade, the geometry of the nacelle and the sleeve. The far wake has less pronounced turbulent vortices, and its length is influenced by more global characteristics of the wind turbine, such as the coefficient of thrust and power, and the conditions of the incoming flow. A decrease in the amount of average kinetic energy (average wind speed) and an increase in turbulence from the downwind side (turbine wakes) affect the processes of heat and moisture exchange and can create cumulative wind effects outside the wind farm. Wind energy losses in wind farms can range from 10 to 20% [6].

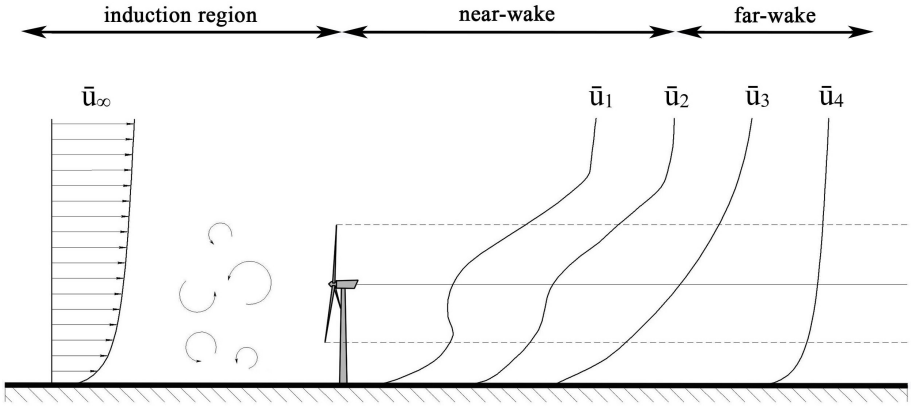


Figure 1. A diagram of the movement of air masses in the area of the wind turbine, showing the flow areas resulting from the interaction of the wind turbine and the incoming turbulent boundary layer.

Cheng Siong Chin, Chu Ming Peh and Mohan Venkateshkumar considered the possibility of modeling offshore wind farms for smart cities [7]. The Jensen model was used in the work, which made it possible to predict the output power taking into account the losses in the wake of the wind turbine. During the construction and operation of a large-capacity wind farm, it is necessary to take into account the influence of the turbulent wake behind the wind turbine and inside the wind farm as a whole, as well as the influence of the turbulent wake on the microclimate due to changes in wind forces. Therefore, it is important to provide scientific methodology and practical data to assess the extent to which wind turbines can affect the local microclimate, especially for practical wind power engineering. Particular attention is paid to the variable parameters of wind turbines: the angular rotational speeds, the yaw angle and the blade pitch angle [8]. Due to the low density of wind energy, increasing the efficiency of converting wind energy into mechanical energy is the main task of increasing the economic efficiency of wind power plants [9–12]. Limited knowledge of wind and turbulence characteristics, taking into account the influence of changes in wind direction in the atmospheric boundary layer (ABL), can affect the reliability of the windproof structure. Many papers have been devoted to wake modeling, in which various tools were used, including the lidar field [13], models based on Taylor theory, as well as Gaussian wake models [14]. The methods used in modeling atmospheric turbulence depend on the features of the considered problems. In the work of B. Lu, it was found that the Coriolis force significantly changes the shape and magnitude of vertical wind velocity profiles in the outer layer of the ABL [15]. In addition, it is now important to study the change in climatic features near wind farms. Lee M. Miller and David W. Keith [16] concluded that wind turbines can increase the surface temperature by 0.24 °C at the regional level as a result of the fact that the turbine rotors mix the air layers close to the ground and redistribute heat and moisture. The wind speed decreases and kinetic energy is removed from the atmosphere. At the regional level, this can lead to drought and affect flora and fauna. Satellite studies have shown that the wake of an offshore wind farm with a capacity of 165 MW can expand downstream up to 55 km, and for a wind farm consisting of 200 turbines with a capacity of 1.5 MW in real terrain with vegetation, the wake flow is deflected downstream by 25 km. Using a numerical experiment for a wind farm consisting

of 100 turbines of 5 MW each, it was found that the wind speed can be restored after 60 km downstream. This indicates that the satellite flow increases as the installed capacity of the wind farm increases. The impact of large wind farms on the local territory is significant, on the regional one—insignificant [17]. For nearby wind farms, the effects of wind farms can lead to a significant decrease in downwind power if buffer zones are not provided [18]. Yu Che and his colleagues proposed a multiscale model of numerical weather prediction (NWP) and a microscale computational fluid dynamics (CFD) model for generating forecasts for the day ahead with high resolution in regions with complex geographical features and variable wind regimes [19]. In the work of D.A. Rayevsky and co-authors, the influence of wind farms on the transition to thermal stratification of the atmosphere of the ABL in the early evening was studied by the example of a wind turbine with a tower height of 120 m. It was revealed that the evening transition within one turbulent wake from a wind turbine began several hours earlier and ended an hour later, the comparison was made with ABL without wind turbines. Changes in temperature stratification due to the creation of turbulence from single turbines can affect the transfer of heat, water and carbon dioxide from surfaces not covered with vegetation, the issue is considered in detail in [20]. With a rapidly growing number of wind turbines, the issue of interaction of turbulence of the ABL with wind turbines, as well as interference effects between turbines, is becoming more acute [21]. A comparison of the simulation results of wind turbines with parallel and offset locations were carried out, which showed a strong influence of the location of wind turbines on the structure of turbulent flow inside and above them. The wind in the lower part of the atmosphere is the most important atmospheric variable; in this area, the greatest wind energy is lost.

The air in the atmosphere is in a state of natural and constant vertical mixing, which is due to atmospheric turbulence, including thermal convection due to the Archimedes force. Wind turbines are intensifiers of temperature stratification of the atmosphere. The stratification of the atmosphere is the distribution of air temperature along the height, characterized by a vertical temperature gradient γ. The stratification of the atmosphere over time cannot be a constant value. For example, on a hot day in the surface layer, the air above the soil heats up and γ increases greatly. At night, the reverse process occurs: the soil heated during the day gives off heat due to convection and the air temperature decreases—sometimes so much that the temperature drop with altitude is replaced by an increase (surface temperature inversion). There are stable and unstable stratification of the atmosphere. With intense convection, turbulent motion and sliding of warm air in the atmosphere (a high value of γ), stratification is unstable. The reverse pattern is observed with stable convection [22]. Wind turbines introduce additional disturbances, increasing γ into the boundary layer of the atmosphere. In [23], the influence of wind turbines on the boundary layer of the atmosphere is considered, the results of comparing the temperature profiles obtained for the base case and the presence of a wind turbine are presented. The movements of the blades enhance vertical mixing and transfer more heat energy from higher levels to lower ones. This leads to an increase in temperature (about 0.5 K) below the level of the upper tip and a decrease between the tip height and the SBL height. For researchers, the study of flows is important, since local meteorology is significantly affected by the general exchange of momentum, heat, moisture, etc.

A large variation in the scale of computational domain is associated with high computational costs; therefore, solving aerodynamics problems on the scale of wind farms has become possible only in recent decades with the development of high-performance computing machines and software such as ANSYS, Fluent, SFX, STAR CCM+, as well as non-commercial packages and other programs. Currently, three methods of mathematical modeling of the atmospheric boundary layer and wind turbines are mainly used. This is the solution of equations averaged by Reynolds (Reynolds-averaged Navier–Stokes (RANS)); vortex-resolving modeling (large eddy simulation (LES)) and direct numerical simulation (DNS) [24–26]. LES can provide reliable and detailed information about the wind turbines wakes, which is necessary to optimize the design of a wind farm (maximizing electricity

generation and minimizing fatigue loads), as well as to adjust more accurate parameters of turbulent flow. In cases where it is necessary to establish an accurate forecast of the flow and its interaction with wind turbines in a wide range of spatial and temporal scales, in order to optimize the placement of wind farms, high precision modeling (HFM) is used, which covers numerical methods of hydrodynamics, ranked according to their processing of turbulence scales and geometric representation. Modeling of wind turbines using HFM is usually divided into three categories: blade resolution models (BRM), actuator line models (ALM) and actuators disk models (ADM) [27].

Recently, numerical simulation of the wind turbine wake has become increasingly popular [28,29]. There are a number of simplified hypotheses about the structure of the flow, among which one can single out Taylor's hypothesis about frozen turbulence: the idea of the cascade transfer of Kolmogorov energy. Currently, many models of weather forecasting and general atmospheric circulation problems and numerical algorithms for their solution have been developed, including using LES [30]. The hierarchy of models "macroscale–mesoscale–microscale" is widespread in modeling. Mathematical modeling of flow parameters in wind farms is performed using the pisoFoamTurbine solver and the actuator-line models method [31]. SOWFA (Simulator for Wind Farm Applications) is a set of computational fluid dynamics (CFD) solvers, boundary conditions and turbine models. It is implemented on the OpenFOAM CFD toolkit and includes a version of the turbine model combined with FAST. This tool is designed to study the performance and load of wind turbines and wind generators in a full range of atmospheric conditions and terrain. Kozin A.A. and Kirpichnikov I.M. developed a model of a wind farm in the MATLAB software package and obtained the characteristics of the operation of a group of wind turbines at the same and different wind speeds [32]. Strizhak S.V. calculated the operation of a single wind turbine using the large eddy simulation and the plane sections along the turbine blade methods. The mathematical model included the basic continuity and momentum equations for an incompressible flow. Large-scale eddy structures were calculated by integrating filtered equations. The calculation was carried out using the Smagorinsky model to determine the value of the turbulent subgrid viscosity [33].

The modeling of a turbulent wake in the thermodynamic boundary layer of the atmosphere is a promising area of research that affects the efficiency of wind power plants and their impact on the climate [34]. A number of studies have been conducted indicating the presence of a turbulent wake behind wind turbines. Studies [35,36] conducted for high-power wind turbines (rated power of 5 MW) show that the route from wind turbines stretched up to 60 km when the wind farm reached the installed capacity. As mentioned above, a change in the structure of the inner boundary layer entails a change in the atmospheric boundary layer, due to high turbulence and vertical mixing of flows, which leads to a change in the gradient of velocity and temperature. Wind turbines can have a long-term impact on local atmospheric conditions [37]. Eugene S. Takle, Daniel A. Rajewski and Samantha L. Purdy [38] noted that the shape, internal characteristics and length of wakes in the wind strongly depend on the thermal stratification of the lower layers of the atmosphere at an altitude of 200 m. Downwind conditions depend on the first turbines and at different altitudes may differ significantly from conditions observed downwind for several turbines.

In most previous studies of flow through isolated wind turbines or wind farms, turbulence parameterization was performed using the RANS, as reflected in the works of K. Alinot, K. Masson, R. Gomez Elvira, A. Crespo, E. Migoya, H. Manuel and F. Hernandez. However, as it has been repeatedly reported in various sources [8], RANS is too dependent on the characteristics of specific streams to be used as a general application method. On the other hand, LES can provide the high-resolution spatial and temporal information needed to maximize wind power generation and minimize wind farm fatigue. There are few works with attempts to use LES for simulation the wind turbine wake [39–42]. Mandar Tabib, Adil Rashid and Trond Kvamsdal applied the LES model of turbulent kinetic energy on a grid scale with one equation and the RANS turbulence model to observe the dynamics of the

wake and power generation at an industrial multi-turbine wind farm. The RANS model predicts higher wind power generation than the LES model because it predicts faster wake attenuation. This is due to the higher turbulence caused by the terrain and the turbulence in the wake predicted by the RANS model [43].

Currently, the existing turbulence models differ from each other in mathematical complexity and, hence, in the required resources for calculations and the accuracy of the description of turbulent processes. When choosing turbulence models for solving industrial problems, researchers often use k-ε turbulence models. Fast convergence, relatively low memory requirements and the cascade solution feature distinguish k-ε turbulence models from the rest. When solving complex problems, modeling of flows with a positive pressure gradient, jet flows and flows in a region with a strongly curved geometry k-ε demonstrates a high error. The model is well suited for solving problems of external flow around bodies of simple geometric shape. For example, the k-ε model can be used to simulate a flow near a poorly streamlined body. Based on the analysis of turbulence models, it is concluded that the k-ε turbulence model will be suitable for solving the problem under consideration. The model under consideration has the feature of a cascade solution, high calculation speed and high accuracy, which makes it possible to use software products with this model on computers that do not have high computing power [44,45].

The conducted research is aimed at studying the processes occurring in the atmospheric boundary layer in the wind turbine zone and studying the turbulent wake, wind energy losses, turbulence and changes in temperature stratification. The research objectives include: (1) assessment of wind potential and features of wind loads in the Ulyanovsk Wind Farm area; (2) proposal of an optimal mathematical model for calculating the atmospheric boundary layer in the wind turbine zone; (3) mathematical modeling and investigation of the characteristics of wind speed and turbulent intensity from the upwind and downwind sides of the wind turbine, using the STAR CCM+ software product; and (4) investigation of the influence of the wind turbine on temperature stratification in the atmospheric boundary layer, based on meteorological observations.

2. Materials and Methods

2.1. Ulyanovsk Wind Farm

The analysis of meteorological observations of the wind farm in the Ulyanovsk region was carried out to study the processes occurring in the atmospheric boundary layer in the wind turbine zone. Based on the obtained data, the initial conditions of the experiment were set. Ulyanovsk Wind Farm has an installed capacity of 85 MW. The wind farm consists of 14 DF2.5 MW-110 turbines and 14 V126-3.45 MW turbines. The location of wind farm is shown in Figure 2).

The wind farm is located on the bank of the Volga River. The direction of the river flow is from north to south. There is a flat terrain in the wind farm area, and the height difference in the wind farm area is 22 m from south to north. The average height of the wind farm relative to sea level is 90.5 m. The area occupied by wind farms is 22.8 km^2. According to [47], south-western and southern winds prevail in the area of the wind farm. The wind rose in the area of the wind farm and the prevailing wind speeds in the region are shown in Figure 3.

The Ulyanovsk region is located in the region of a temperate continental climate zone with a forest–steppe zone. Figure 4 shows the annual wind speed for 2020.

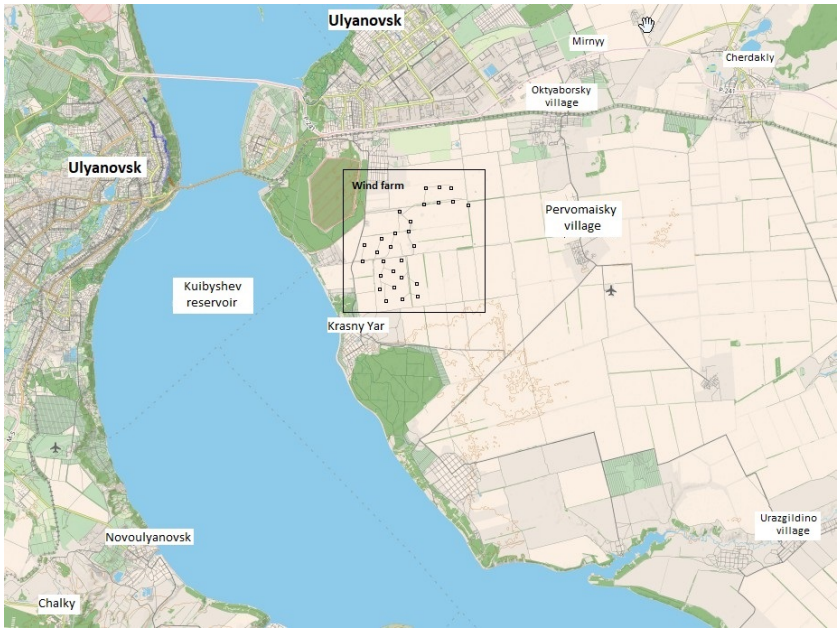


Figure 2. Ulyanovsk Wind Farm (photo from [46]).

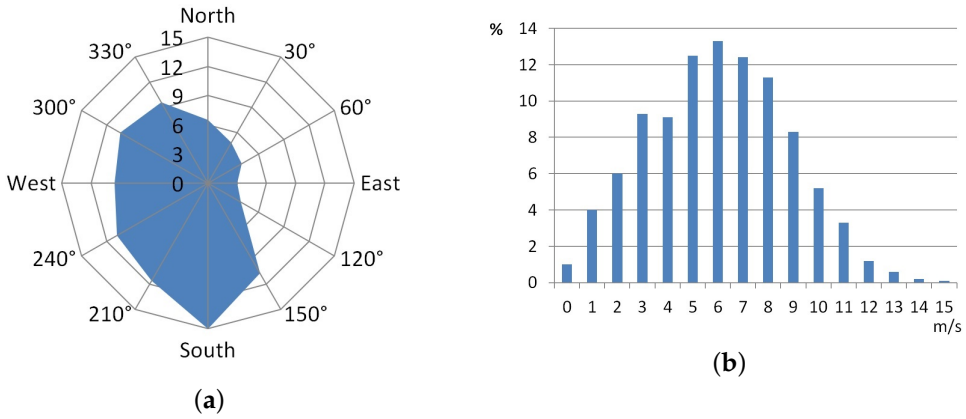


Figure 3. Wind data for 2020 at an altitude of 100 m from the surface. (**a**) The average annual wind rose; (**b**) the average annual wind speed in the wind farm area.

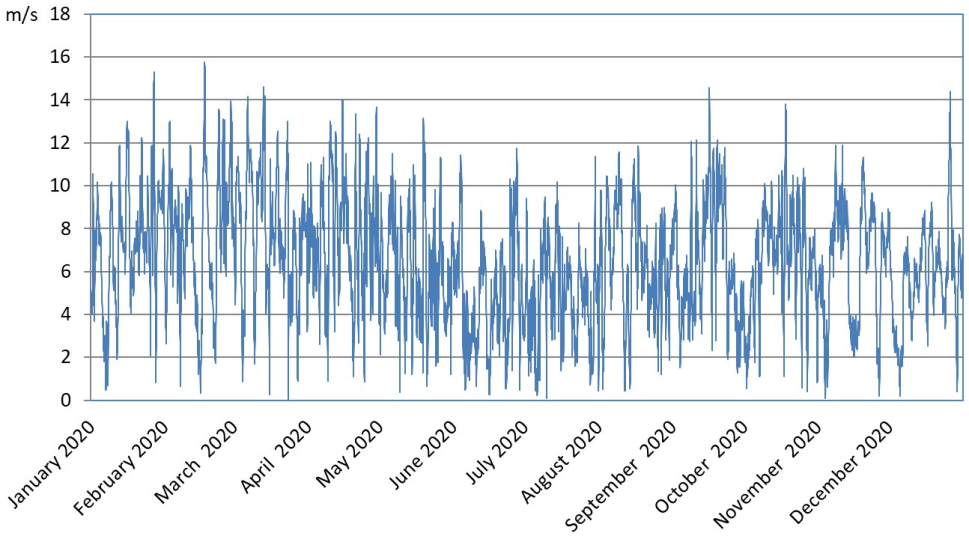


Figure 4. Distribution of wind speed in the wind farm zone at an altitude of 100 m.

The climate of the Ulyanovsk region is characterized by moderately cold winters and warm summers, formed under the influence of continental air of temperate latitudes. A short dry spring is a feature of the climate. Autumn in the Ulyanovsk region is usually warm; snow is established in the second half of November. The coldest month is January. Winter is snowy, with frequent temperature changes (Atlantic cyclones are replaced by Arctic air masses and vice versa), and lasts from mid-November to mid-March. The average long-term temperature in January ranges from −12.5 °C to −14 °C, where the absolute minimum temperature in winter is −48 °C. Summer weather is set in mid-May. Summers are usually hot due to the influence of sedentary Asian anticyclones. The average monthly temperature in July ranges from +18.6 °C to +20.4 °C, and the absolute maximum temperature in summer was +41 °C. Precipitation ranges from 350 mm in the south of the region to 500 mm in the northwest. In summer, precipitation falls unevenly in the form of heavy and short-term rains.

2.1.1. Mathematical Model of the Atmospheric Boundary Layer in the Wind Turbine Zone

We use the commercial package STAR CCM+ with an integrated module for optimizing the operation of the wind farm, taking into account the orography of the surface, the polydispersity of the flow, as well as the pressure gradient. STAR CCM+ uses the built-in RANS equations for calculation, and the *k*-ε turbulence model was used to close the system of equations. The RANS method is widely used in the calculation of practical problems, providing high convergence and accuracy, while spending less power compared to LES and especially DNS methods.

The statement of the mathematical problem is formulated in the form:

– Continuity equation:

$$\frac{\partial \rho}{\partial t} + \frac{\partial (\rho u_i)}{\partial x_i} = 0, \tag{1}$$

where ρ is the air density, [kg/m^3]; x_i is the coordinates in the i-direction (corresponding to the streamwise, spanwise and vertical directions), [m]; u_i is the resolved velocity in the i-direction, [m/s].

– Equation of motion:

$$\frac{\partial (\rho u_i)}{\partial t} + \frac{\partial (\rho u_i u_j)}{\partial x_i} = -\frac{\partial P}{\partial x_i}\left[\mu\left(\frac{\partial u_i}{\partial x_i}\partial x_j - \frac{\partial u_j}{\partial x_i} - \frac{2}{3}\delta_{i,j}\frac{\partial u_k}{\partial x_k}\right)\right] - \frac{\partial (\rho \overline{u_i' u_j'})}{\partial x_i} + \rho g_i, \tag{2}$$

where P is the pressure, [Pa], u_i' is pulsation component of the velocity, m/s.

– Energy equation:

$$\frac{\partial (\rho h)}{\partial t} + \frac{\partial (\rho u_i h)}{\partial x_i} = \frac{\partial}{\partial x_i}\left(\lambda + c_p \frac{\mu_t}{Pr_t}\right)\frac{\partial T}{\partial x_i}, \tag{3}$$

where h is the enthalpy, [kJ/kg], defined as

$$h = c_p T; \tag{4}$$

c_p is the specific isobaric heat, [kJ/kg*K]; T is the air temperature, [K]; λ is the heat transfer coefficient, [W/(m*K)]; μ_t is the turbulent viscosity coefficient; Pr_t is the turbulent Prandtl number, Pr_t = 0.85, $\frac{\partial T}{\partial x_i}$ is the temperature stratification of the atmosphere [15].

To describe the turbulence of the flow, the standard *k*-ε model:

$$\frac{\partial (\rho k)}{\partial t} + \frac{\partial (\rho k u_i)}{\partial x_i} = -\frac{\partial}{\partial x_i}\left[\left(\mu + \frac{\mu_t}{\sigma_k}\right) grad\ k\right] + 2\mu_t E_{ij} E_{ij} + G_b - \rho\varepsilon + S_k, \tag{5}$$

where k is the turbulent kinetic energy; E_{ij} is the stress tensor defined by standard *k*-ε models; S_k is the source term, defined as:

$$S_k = -\beta g_i^2 \frac{\mu_t}{c_p Pr_t} \tag{6}$$

where G_b is the generation of turbulence due to temperature stratification, defined as:

$$G_b = \beta\, g_i \frac{\mu_t}{Pr_t} \frac{\partial T}{\partial x_i}, \tag{7}$$

where β is the coefficient of thermal expansion, [1/K]; g_i is the component of the gravity vector in the i-th direction for ideal gases. Equation (7) takes the form:

$$G_b = -g_i \frac{\mu_t}{\rho Pr_t} \frac{\partial P}{\partial x_i}; \tag{8}$$

– Dissipation of turbulent kinetic energy of turbulence equation:

$$\frac{\partial(\rho\varepsilon)}{\partial t} + \frac{\partial(\rho\varepsilon u_i)}{\partial x_i} = \frac{\partial}{\partial x_i}\left[\left(\mu + \frac{\mu_t}{\sigma_\varepsilon}\right) grad\varepsilon\right] + C_{1\varepsilon}\frac{\varepsilon}{k}\left(2\mu_t E_{ij}E_{ij} + C_{3\varepsilon}G_b\right) - C_{2\varepsilon}\rho\frac{\varepsilon^2}{k} + S_\varepsilon, \tag{9}$$

where ε is the rate of dissipation of turbulent kinetic energy; S_ε is the source term, assumed to be 0; $C_{1\varepsilon}$ = 1.176, $C_{2\varepsilon}$ = 1.92, $C_{3\varepsilon}$ are the empirical constants.

Constant $C_{3\varepsilon}$ depends on the Archimedean force and is determined by

$$C_{3\varepsilon} = \tan h \frac{u_j}{u_i}. \tag{10}$$

The turbulent viscosity is determined by the expression:

$$\mu_t = \rho C_\mu \frac{k^2}{\varepsilon}. \tag{11}$$

The coefficient of turbulent diffusion is determined by the expression:

$$\Gamma_t = \frac{\mu_t}{Sc_t}. \tag{12}$$

– Equation of state:

$$\rho = \frac{P}{RT}. \tag{13}$$

where R is the gas constant.

Turbulence constants, based on sources [15,18,19], it is acceptable to accept equal

$$C_\mu = 0.0333; \sigma_k = 1.00; \sigma_\varepsilon = 1.3; \tag{14}$$

Boundary conditions for stationary ABL:

$$\frac{\partial\rho}{\partial t} = 0; \quad \frac{\partial(\rho u_i)}{\partial t} = 0; \quad \frac{\partial(\rho h)}{\partial t} = 0; \tag{15}$$

$$\frac{\partial(\rho k)}{\partial t} = 0; \quad \frac{\partial(\rho\varepsilon)}{\partial t} = 0; \quad C = 0; \tag{16}$$

The rotation of the wind turbine blades is set by the rotation of the moving grid. The profile of wind speed varies in height according to the power law, temperature—in a linear law. The system of Equations (1)–(13) with boundary conditions (15) and constants (14) is solved with respect to the components of velocity, temperature and turbulent characteristics.

At given rotational speeds, the optimal operating mode of the turbine is characterized by the highest power coefficient, the Betz criterion ξ, which depends on the coefficient of friction resistance on the wind blade surface.

$$C_f = \frac{\xi}{8} = \frac{\tau_w}{u^2} \quad (17)$$

where C_f, ξ are the coefficients of friction resistance, and τ_w is the turbulent friction stress.

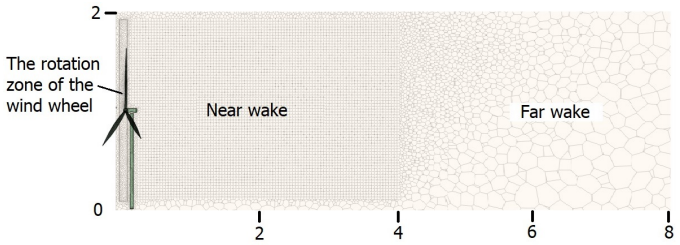
2.1.2. Mesh Scene and Experimental Conditions

The commercial product STAR CCM+ was used to design the wind turbine and the working domain. A 3D CAD model of the DF2.5 MW-110 wind turbine on a one-to-one scale was created. Polyhedral mesh was used for a more accurate calculation with the allocation of special study zones, such as: the rotation zone of the rotor, the near wake zone and the wind tunnel (see Figure 5). The mesh sizes are chosen to obtain sufficient accuracy and minimize the computational time spent on the computer. The study of gas-dynamic characteristics in the area of the wind wheel is a fundamental factor for accurate calculation of the air flow in the study area; therefore, a mesh with a step of 0.01 m was used. In the zone of the near wake, a mesh with a step of 0.08 m was used, based on the recommendations presented in the works of other researchers. In the far wake area, a mesh with a step of 5 m was used, which makes it possible to efficiently calculate hydrogeodynamic processes with sufficient accuracy for evaluation. The total number of cells was 2,343,830. Using the built-in capabilities of the program, the mesh steps y+ were checked, the obtained values <1, which corresponds to the correct choice of the mesh. To verify the adequacy of the solutions obtained, a comparison was made with the results of other researchers [5].

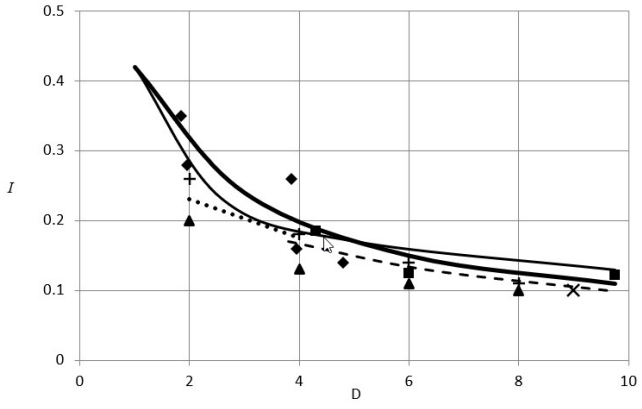
The computational domain was limited to two rotor diameters in height and eight diameters in length (see Figure 6). The wind speed from the upwind side was set to gradient, with a maximum value of 12 m/s, as close as possible to the real data obtained from observations [47]. The upper and side walls of the wind tunnel were set as isosurfaces, the lower surface had roughness to increase the friction resistance on the wall C_f = 0.008. Simulation of the wind turbine operation was performed within 25 s, which made it possible to bring the non-stationary process to the constancy of values.

The Y+ parameter is one of the main parameters in hydro-gas dynamics, the parameter that determines the correctness of the calculated grid. Looking ahead, we immediately note that, after the calculations, the value of the parameter y+ on the solid walls of the calculation area must be checked. The grid should be small enough near the walls to resolve the boundary layer phenomenon, but large enough to be solved on the available computing resources. Figure 7 shows the results of the correctness of the calculated grid on the blades of the wind generator.

The k-ε model does not require excessive grinding of the mesh near a solid surface. For the selected turbulence model, adequate results are obtained at Y+ $\leq$ 1, based on the tutorial STAR CCM+. Y+ is the dimensionless distance from the wall to the center of the cell adjacent to the wall.



(**a**)



(**b**)

Figure 5. (**a**) Mesh scene area diagram; (**b**) Comparison of the turbulence intensity in the wake at the hub height, measured in four different clusters of wind turbines, is done with the model used, as well as the Quarton model and the Crespo and Hernandez model, 9 m/s < U < 11 m/s: solid line—Frandsen and Thogersen [5]; solid thin line—Qarton [5]; dotted line—Crespo and Hernandez [5]; ■—Alsvik [5]; ×—Vindeby [5]; •—Taff Ely [5]; ♦—Andros [5]; ▲—turbulence intensity without a dedicated near wake in the calculated area, +—turbulence intensity with a dedicated near wake in the calculated area.

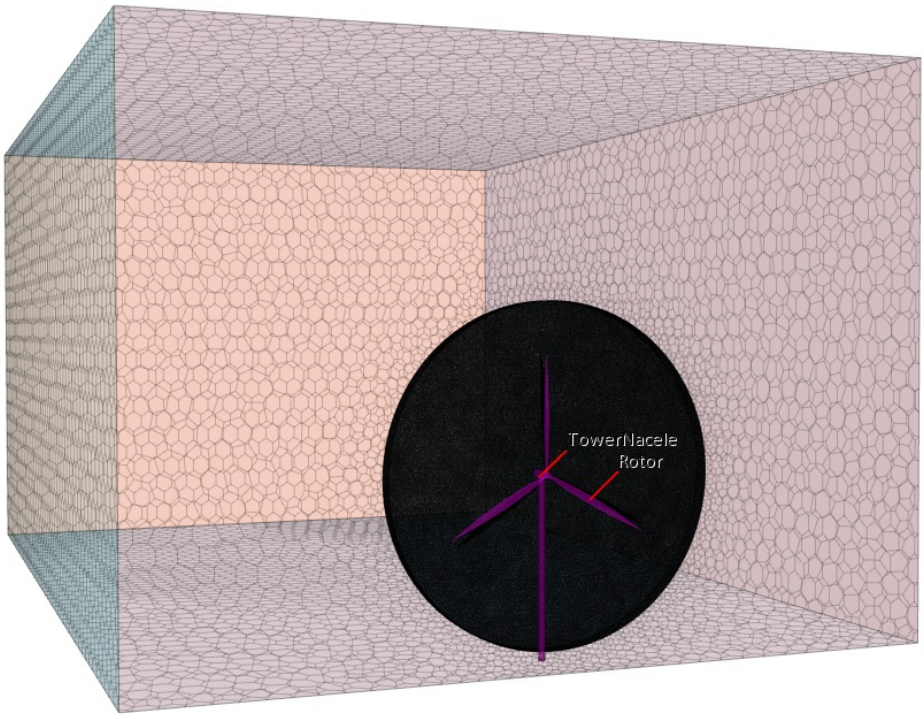
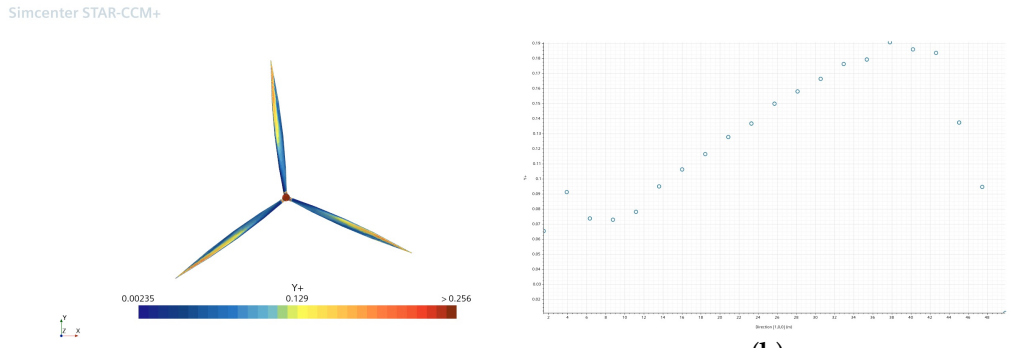


Figure 6. The wind tunnel mesh scene.

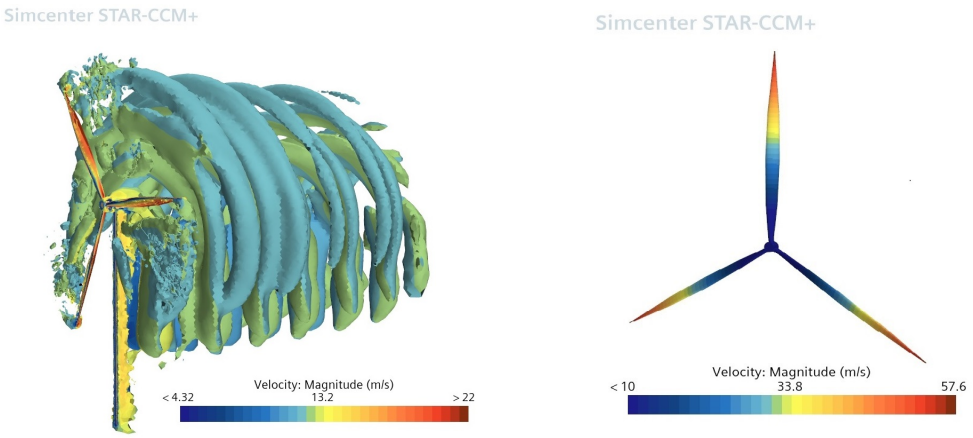


(**a**) (**b**)

Figure 7. Distribution of the Y+ value on the wind turbine blades. (**a**) 3D model, (**b**) graph.

3. Research Results and Discussion

A study of the turbulent wake behind the wind turbine, geometrically similar to DF2.5 MW-110, whose rated power develops at a wind speed of 10.5 m/s [48], was carried out based on known data on the terrain of the Ulyanovsk Wind Farm and the properties of the atmospheric boundary layer. The commercial package STAR CCM+ [49] was used for the study, which includes a set of methods and models for calculating gas dynamics and stratification. The RANS method and the standard *k*-ε turbulence model were used to model a single wind turbine and study its turbulent wake. The formed near wake behind the wind turbine and the velocity distribution on the blades of the wind turbine is shown in Figure 8.



(**a**) (**b**)

Figure 8. Research results: (**a**) wake behind the wind turbine, (**b**) velocity distribution on the blades of the wind turbine.

The near-wake region is characterized by high turbulence and the greatest change in the velocity gradient. The blades of the wind turbine leave significant disturbances in the near wake in the form of sinusoidal vortices. A high concentration of turbulent vortices is observed behind the turbine, which is also visible at the end of the near wake.

Figure 9 shows the results of modeling the speed gradient before and behind the wind turbine, and the graph also show speed losses (the difference between the initial speed before the wind turbine and the final speed in the plane section after the wind turbine). The speed difference allows you to estimate the loss and recovery of wind energy.

Four points were selected from the downwind side at a distance of D = 2, D = 4, D = 6, D = 8 (D is the distance in diameters of the wind turbine blades) from the wind turbine mast to illustrate the restoration of the velocity gradient behind the wind turbine. The experiment showed that the wind turbine leaves a significant wake on the nominal

load parameters, which is capable of causing a decrease in the power of subsequent wind turbines. At a distance of D = 8 from the mast of the wind turbine, the average speed over the simulated cross-section is reduced by 0.6 m/s.

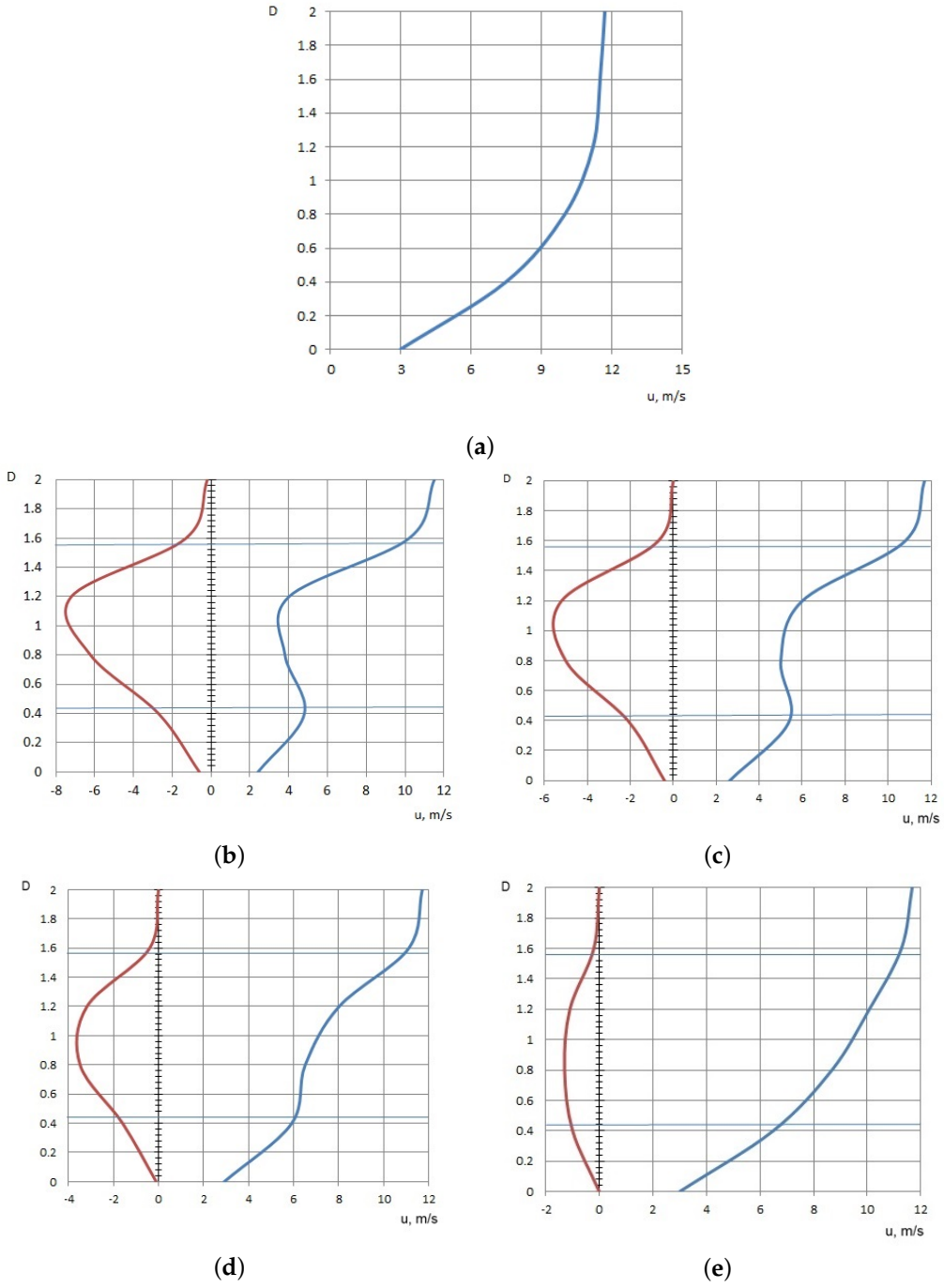


Figure 9. Velocity gradients before and behind the wind turbine. (**a**) velocity gradient before the wind turbine; (**b**) velocity gradient behind the wind turbine at D = 2; (**c**) velocity gradient behind the wind turbine at D = 4; (**d**) velocity gradient behind the wind turbine at D = 6; (**e**) velocity gradient behind the wind generator at D = 8 (D is the distance in diameters of the wind turbine blades).

The turbulence intensity was also estimated $\sigma_u/\overline{u}$ in the impact zone of the wind turbine. Figure 10 shows the results of modeling the turbulence profile in the wind turbine zone.

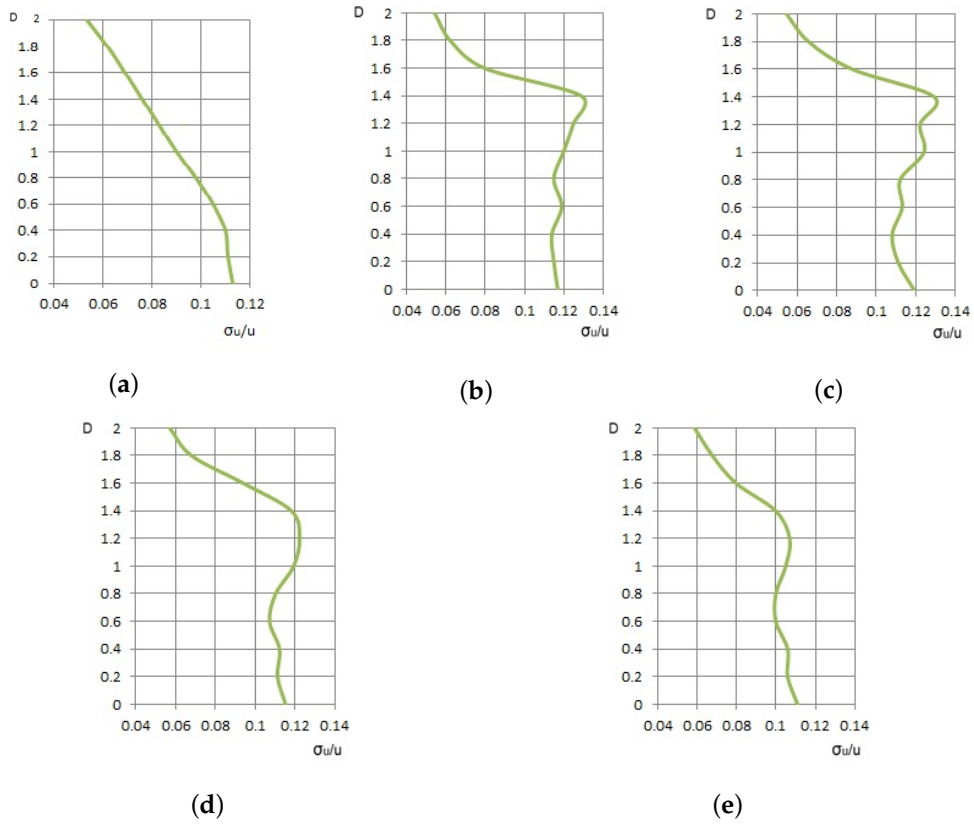


Figure 10. Profile of the turbulent intensity in the wind turbine zone: (**a**) intensity of turbulence before the wind turbine; (**b**) intensity of turbulence behind the wind generator at D = 2; (**c**) the intensity of turbulence behind the wind generator at D = 4; (**d**) the intensity of turbulence behind the wind generator at D = 6; (**e**) the intensity of turbulence behind the wind generator at D = 8.

The data presented in Figure 10, showing the intensity of turbulence, are obtained in the same sections as the velocity gradients (D = 2, D = 4, D = 6, D = 8). The wind turbine in the process of operation takes significant energy from the wind flow, and introduces significant disturbances, which affects the pulsation of the longitudinal and transverse velocity behind the wind generator. Analyzing the presented profiles, it should be noted that the disturbance introduced by the wind turbine remains noticeable at a distance of D = 8, while the percentage ratio taken from the average turbulence intensity in the cross section is 8.24% higher than in the cross section in front of the wind generator. A study of the boundary air layer of the atmosphere with a temperature at the earth's surface of 298.3 K (30 July 2020 03.00 p.m.) was carried out to analyze the effect of a single wind turbine on temperature stratification. Data on the temperature gradient were taken from [47]. The results of modeling the temperature stratification of the boundary layer in the wind turbine zone are shown in Figure 11.

An increase in turbulence in the boundary layer irreversibly leads to a redistribution of air temperature along the height as a result of mixing flows. As discussed earlier, wind turbines are artificial turbulators that cause a significant change in the gradient of velocity and energy in the atmospheric boundary layer. The impact of a single wind turbine is expressed in a slight change in temperature (up to 0.5 K). However, it should be noted that when considering wind farms, temperature stratification will undergo more significant changes; in addition, nighttime changes in temperature, humidity and pressure will have an impact.

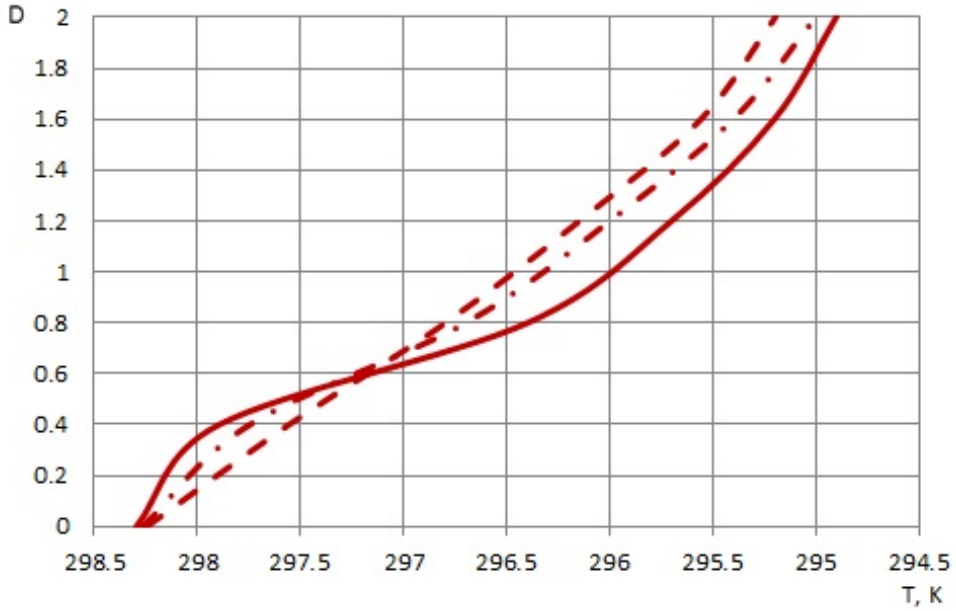


Figure 11. Temperature stratification of the boundary layer in the wind turbine zone: solid line—without wind turbine; dotted line—temperature stratification at a distance D = 4 from the mast of the wind turbine; dot-dash line—temperature stratification at a distance D = 8 from the mast of the wind turbine.

4. Conclusions

The article presents the results of mathematical modeling of the of the atmospheric boundary layer in the wind turbine zone, taking into account temperature and velocity gradients. The paper used the RANS equations for calculation, and the k-ε turbulence model was used to close the system of equations. The RANS method is widely used in the calculation of practical problems, providing high convergence and accuracy, while spending less power compared to LES and especially DNS methods.

When studying the wind speed in the wind turbine zone, it was found that the wind turbine leaves a significant wake at the nominal load parameters, even at a distance of D = 8 from the mast of the wind turbine. With the quantitative data, we would like to note a decrease in the average speed by 0.6 m /s in the last section D = 8, compared with the initial speed to the wind turbine, which will lead to a decrease in the power of wind turbines falling into the wake region up to 6%.

The results obtained during the study of the intensity of turbulence in the wind turbine wake show a significant change in the longitudinal velocity behind the turbine. Turbulent wind flow leads to premature failure of wind turbines due to the resulting uneven loads and vibrations. Analyzing the presented profiles, it should be noted that the disturbance introduced by the wind turbine remains noticeable at a distance of D = 8, while the percentage ratio taken from the average turbulence intensity in the cross section is 8.24% higher than in the cross section in front of the turbine. When considering the changes in temperature stratification during the interaction of the boundary layer with wind turbines, it is possible to note a slight change in temperature (up to 0.5 K), which is insignificant, but at night the value can reach large values.

The wind turbines of the Ulyanovsk Wind Farm are located at a distance of 700–900 m from each other, which means that some of the turbines will fall into the long-range wake when they reach their rated power. Considering the prevalence of south-western and southern winds in the wind farm region, a number of wind turbines can be identified, falling within the range of the far wake of wind turbine. A percentage of 10.6% is the share of winds per year at which wind turbines operate at nominal parameters; therefore, in this mode, the received power will be reduced to 6% for part of the wind turbines.

Author Contributions: Conceptualization, V.N.K., R.V.F. and A.V.C.; methodology, V.N.K., R.V.F. and A.V.C.; software, A.V.C., E.V.T. and M.I.K.; validation, E.V.T. and M.I.K.; investigation, V.N.K., R.V.F. and A.V.C.; writing—original draft preparation, V.N.K., R.V.F. and A.V.C.; writing—review and editing, V.N.K., R.V.F. and A.V.C.; visualization, A.V.C., E.V.T. and M.I.K.; supervision, V.N.K.; project administration, R.V.F.; funding acquisition, R.V.F. All authors have read and agreed to the published version of the manuscript.

Funding: The research was carried out by the grant of the Russian Science Foundation No. 22-19-00030, https://rscf.ru/project/22-19-00030 (accessed on 11 September 2022).

Data Availability Statement: Not applicable.

Conflicts of Interest: The authors declare no conflict of interest.

Nomenclature

i, j, k	direction corresponding to the streamwise, spanwise and vertical directions
x_i	coordinates in the i-direction, m
u_i	resolved velocity in the i-direction, m/s
u_i'	pulsation component of the velocity in the i-direction, m/s
P	pressure, Pa
T	air temperature, K
ρ	air density, kg/m^3
h	enthalpy, kJ/kg
c_p	specific isobaric heat, kJ/kg*K
λ	heat transfer coefficient, W/(m*K)
μ_t	turbulent viscosity coefficient
k	turbulent kinetic energy
E_{ij}	stress tensor defined by standard k-ε models
S_k	source term
C_f, ξ	coefficients of friction resistance
τ_w	turbulent friction stress
D	distance in diameters of the wind turbine blades
Abbreviations	
CAD	computer aided design
CFD	computational fluid dynamics
ABL	atmospheric boundary layer
NWP	numerical weather prediction
RANS	Reynolds-averaged Navier–Stokes
LES	large eddy simulation
DNS	direct numerical simulation
HFM	high precision modeling
BRM	blade resolution models
ALM	actuator line models
ADM	actuators disk models
SOWFA	simulator for wind farm applications

References

1. Stepanov, V.S.; Stepanova, T.B.; Starikova, A.A. Sistemnyi analiz tselesoobraznosti sozdaniya lokal'nykh energosistem [System analysis of the expediency of creating local power supply systems]. *Sovremennye tekhnologii Sistemnyi analiz Modelirovanie [Mod. Technol. Syst. Anal. Model.]* **2018**, *60*, 117–124. (In Russian)
2. Narbel, P.A.; Hansen, J.P. Estimating the cost of future global energy supply. *Renew. Sustain. Energy Rev.* **2014**, *34*, 91–97. [CrossRef]
3. Medici, D.; Ivanell, S.; Dahlberg, J.Å.; Alfredsson, P.H. The upstream flow of a wind turbine: Blockage effect. *Wind Energy* **2011**, *14*, 691–697 [CrossRef]
4. Porté-Agel, F.; Bastankhah, M.; Shamsoddin, S. Wind-Turbine and Wind-Farm Flows: A Review. *Bound.-Layer Meteorol* **2020**, *174*, 1–59. [CrossRef] [PubMed]
5. Vermeer, L.J.; Sørensen, J.N.; Crespo, A. Wind turbine wake aerodynamics. *Prog. Aerosp. Sci.* **2003**, *39*, 467–510. [CrossRef]
6. van der Laan, M.P.; Sørensen, N.N.; Réthoré, P.-E.; Mann, J.; Kelly, M.C.; Troldborg, N.; Schepers, J.G.; Machefaux, E. An improved k-ε model applied to a wind turbine wake in atmospheric turbulence. *Wind Energy* **2015**, *18*, 889–907. [CrossRef]

7. Chin, C.; Peh, C.; Venkateshkumar, M. Modeling and Simulation of Offshore Wind Farms for Smart Cities In *Modeling, Simulation and Optimization of Wind Farms and Hybrid Systems*; Maalawi, K.; IntechOpen: London, UK, 2020.
8. Ivanov, A.V.; Strijhak, S.V.; Zakharov, M.I. Modeling weather conditions in the port area and coastal zone of Tiksi Bay. *Proc. Inst. Syst. Program. RAS (Proc. ISP RAS)* **2019**, *31*, 163–176. (In Russian) [CrossRef]
9. Porté-Agel, F.; Wu, Y.-T.; Lu, H.; Conzemius, R.J. Large-eddy simulation of atmospheric boundary layer flow through wind turbines and wind farms. *J. Wind. Eng. Ind. Aerodyn.* **2011**, *99*, 154–168. [CrossRef]
10. Hsieh, A.S.; Brown, K.A.; deVelder, N.B.; Herges, T.G.; Knaus, R.C. High-fidelity wind farm simulation methodology with experimental validation. *J. Wind. Eng. Ind. Aerodyn* **2021**, *218*, 104754. [CrossRef]
11. Ichenial, M.M.; El-Hajjaji, A.; Khamlichi, A. Modeling of the atmospheric boundary layer under stability stratification for wind turbine wake production. *Wind Eng.* **2021**, *45*, 178–204. [CrossRef]
12. Goit, J.P.; Meyers, J. Optimal control of energy extraction in wind-farm boundary layers. *J. Fluid Mech.* **2015**, *768*, 5–50. [CrossRef]
13. Annoni, J.; Fleming, P.; Scholbrock, A.; Roadman, J.; Dana, S.; Adcock, C.; Porte-Agel, F.; Raach, S.; Haizmann, F.; Schlipf, D. Analysis of control-oriented wake modeling tools using lidar field results. *Wind. Energy Sci.* **2018**, *3*, 819–831. [CrossRef]
14. Vahidi, D.; Porté-Agel, F. A physics-based model for wind turbine wake expansion in the atmospheric boundary layer. *J. Fluid Mech.* **2022**, *943*, A49. [CrossRef]
15. Lu, B.; Li, Q.-S. Large eddy simulation of the atmospheric boundary layer to investigate the Coriolis effect on wind and turbulence characteristics over different terrains. *J. Wind. Eng. Ind. Aerodyn.* **2022**, *220*, 104845. [CrossRef]
16. Miller, L.M.; David, W.K. Climatic impacts of wind power. *Joule 2* **2018**, *12*, 2618–2632. [CrossRef]
17. Wang, Q.; Luo, K.; Wu, C.; Fan, J. Impact of substantial wind farms on the local and regional atmospheric boundary layer: Case study of Zhangbei wind power base in China. *Energy* **2019**, *183*, 1136–1149. [CrossRef]
18. Wang, Q.; Luo, K.; Wu, C.; Zhu, Z.; Fan, J. Mesoscale simulations of a real onshore wind power base in complex terrain: Wind farm wake behavior and power production. *Energy* **2022**, *241*, 122873. [CrossRef]
19. Yuzhang, C.; Andrés, A.S.; Siyue, P.; Jiafeng, Z.; Yangruixue, C.; Liang, Y. A multi-scale model for day-ahead wind speed forecasting: A case study of the Houhoku wind farm, Japan. *Sustain. Energy Technol. Assessments* **2022**, *52*, 101995.
20. Rajewski, D.A.; Takle, E.S.; Lundquist, J.K.; Prueger, J.H.; Pfeiffer, R.L.; Hatfield, J.L.; Spoth, K.K.; Doorenbos, R.K. Changes in fluxes of heat, H_2O, and CO_2 caused by a large wind farm. *Agric. For. Meteorol.* **2014**, *194*, 175–187. [CrossRef]
21. Bastankhah, M.; Porté-Agel, F. Wind farm power optimization via yaw angle control: A wind tunnel study. *J. Renew. Sustain. Energy* **2019**, *11*, 023301. [CrossRef]
22. Kurgansky, M.V.; Krupchatnikov, V.N. Research in dynamic meteorology in Russia in 2015–2018. *Proc. Russ. Acad. Sci. Phys. Atmos. Ocean* **2019**, *55*, 6–47.
23. Porté-Agel, F.; Lu, H.; Wu, Y.-T. Interaction between large wind farms and the atmospheric boundary layer. *Procedia IUTAM* **2014**, *10*, 307–318. [CrossRef]
24. Calaf, M.; Meneveau, C.; Meyers, J. Large Eddy Simulation Study of Fully Developed Wind-turbine Array Boundary Layers. *Phys. Fluids* **2010**, *22*, 1–16. [CrossRef]
25. Martínez-Tossas, L.A.; Churchfield, M.J.; Leonardi, S. Large eddy simulations of the flow past wind turbines: Actuator line and disk modeling. *Wind Energy* **2015**, *18*, 1047–1060. [CrossRef]
26. Mehta, D.; Van Zuijlen, A.H.; Koren, B.; Holierhoek, J.G.; Bijl, H. Large Eddy Simulation of wind farm aerodynamics: A review. *J. Wind. Eng. Ind. Aerodyn.* **2014**, *133*, 1–17. [CrossRef]
27. Jha, P.K.; Churchfield, M.J.; Moriarty, P.J.; Schmitz, S. Guidelines for Volume Force Distributions Within Actuator Line Modeling of Wind Turbines on Large-Eddy Simulation-Type Grids. *ASME J. Sol. Energy Eng.* **2014**, *136*, 031003. [CrossRef]
28. Abdelsalam, A.M.; Ramalingam, V. Numerical simulation of atmospheric boundary layer and wakes of horizontal-axis wind turbines. *J. Energy South. Afr.* **2017**, *25*, 44–50. [CrossRef]
29. Lundquist, J.K.; Churchfield, M.J.; Lee, S.; Clifton, A. Quantifying error of lidar and sodar Doppler beam swinging measurements of wind turbine wakes using computational fluid dynamics. *Atmos. Meas. Tech.* **2015**, *8*, 907–920 [CrossRef]
30. Abkar, M.; Porté-Agel, F. Influence of atmospheric stability on wind-turbine wakes: A large-eddy simulation study. *Phys. Fluids* **2015**, *27*, 035104. [CrossRef]
31. Kraposhin, M.V.; Strijhak, S.V. The problem-oriented library SOWFA for solving the applied tasks of wind energy. *Proc. Inst. Syst. Program. RAS (Proc. ISP RAS)* **2018**, *30*, 259–274. (In Russian) [CrossRef]
32. Kozin, A.A.; Kirpichnikova, M. Analysis of the group of vertical-axis wind turbines in the software package MATLAB. *Altern. Energy Ecol. (ISIEE)* **2014**, *5*, 45–49.
33. Strijhak, S.V. Mathematical modeling of flow parameters for single wind turbine. *Civ. Aviat. High Technol.* **2016**, *19*, 176–184. (In Russian)
34. Koshelev, K.B.; Strihhak, S.V. Simulation of particle dynamics in planetary boundary layer and in a model wind farm. *Proc. Inst. Syst. Program. RAS (Proc. ISP RAS)* **2019**, *31*, 177–186. (In Russian) [CrossRef]
35. Fitch, A.C.; Olson, J.B.; Lundquist, J.K.; Dudhia, J.; Gupta, A.K.; Michalakes, J.; Barstad, I. Local and mesoscale impacts of wind farms as parameterized in a mesoscale NWP model. *Mon. Weather. Rev.* **2012**, *140*, 3017–3038. [CrossRef]
36. Fitch, A.C.; Lundquist, J.K.; Olson, J.B. Mesoscale influences of wind farms throughout a diurnal cycle. *Mon. Weather. Rev.* **2013**, *141*, 2173–2198. [CrossRef]

37. Bodini, N.; Lundquist, J.K.; Moriarty, P. Wind plants can impact long-term local atmospheric conditions. *Sci. Rep.* **2021**, *11*, 22939. [CrossRef]
38. Takle, E.S.; Rajewski, D.A.; Purdy, S.L. The Iowa Atmospheric Observatory: Revealing the Unique Boundary-Layer Characteristics of a Wind Farm. *Earth Interact.* **2019**, 23, 1–27. [CrossRef]
39. Lu, H.; Porté-Agel, F. Large-eddy simulation of a very large wind farm in a stable atmospheric boundary layer. *Phys. Fluids* **2011**, *23*, 065101. [CrossRef]
40. Wu, Y.T.; Porté-Agel, F. Large-eddy simulation of wind-turbine wakes: Evaluation of turbine parametrisations. *Bound.-Layer Meteorol.* **2011**, *138*, 345–366. [CrossRef]
41. Revaz, T.; Porté-Agel, F. Large-Eddy Simulation of Wind Turbine Flows: A New Evaluation of Actuator Disk Models. *Energies* **2021**, *14*, 3745. [CrossRef]
42. Breton, S.P.; Sumner, J.; Sørensen, J.N.; Hansen, K.S.; Sarmast, S.; Ivanell, S. A survey of modelling methods for high-fidelity wind farm simulations using large eddy simulation. *Philos. Trans. R. Soc. A Math. Phys. Eng. Sci.* **2017**, *375*, 20160097. [CrossRef] [PubMed]
43. Tabib, M.; Rasheed, A.; Kvamsdal, T. LES and RANS simulation of onshore bessaker wind farm: Analysing terrain and wake effects on wind farm performance. *J. Phys. Conf. Ser.* **2017**, *625*, 012032. [CrossRef]
44. Li, N.; Liu, Y.; Li, L.; Chang, S.; Han, S.; Zhao, H.; Meng, H. Numerical simulation of wind turbine wake based on extended k-epsilon turbulence model coupling with actuator disc considering nacelle and tower. *IET Renew. Power Gener.* **2020**, *14*, 3834–3842. [CrossRef]
45. Baungaard, M.; van der Laan, M.P.; Kelly, M. RANS modeling of a single wind turbine wake in the unstable surface layer. *Wind Energ. Sci.* **2022**, *7*, 783–800. [CrossRef]
46. OpenStreetMap. Available online: https://www.openstreetmap.org/#map=15/54.2843/48.5974&layers=Y (accessed on 11 September 2022).
47. Weather and Climate—Weather Forecasts, Weather News, Climate Data. Available online: http://www.pogodaiklimat.ru (accessed on 11 September 2022).
48. Dongfang Electric Corporation (DEC). Available online: http://www.dongfang.com.cn (accessed on 11 September 2022).
49. Star CMM+ Singapore. Available online: https://star-ccm.com (accessed on 11 September 2022).